AIAA JOURNAL
Vol. 31, No. 4, April 1993

Analysis of Delamination Initiation in Postbuckled Dropped-Ply Laminates

Carlos G. Dávila*
NASA Langley Research Center, Hampton, Virginia 23665
and
Eric R. Johnson†
Virginia Polytechnic Institute and State University, Blacksburg, Virginia 24061

The compression strength of dropped-ply, graphite-epoxy laminated plates for the delamination mode of failure is studied by a finite element analysis and corroborated with experiments. The compression strength of the 2.54-cm-wide specimens, which exhibited a linear response to delamination initiation, is greater than the compression strength of the 7.62-cm-wide specimens with the same layup, which exhibited a nonlinear response to delamination. Analyses confirm that the influence of the geometric nonlinearity on the response of the 2.54-cm-wide dropped-ply laminate is insignificant, but this nonlinearity is very significant in the response of its 7.62-cm-wide counterpart. For the 7.62-cm-wide dropped-ply laminate, the decrease in compression strength is associated with the redistribution and intensification of the severe interlaminar stress gradients occurring at the dropoff to a location closer to the knife-edge support.

Introduction

TERMINATING internal plies, or dropping plies, is an effective method of stiffness tailoring for laminated structures. However, the abrupt thickness change at the ply dropoff causes a stress riser that may limit the strength. Some studies on the response and/or failure of dropped-ply laminates under static uniaxial loading perpendicular to the ply termination are given in Refs. 1–6. These include symmetric dropped-ply laminates loaded in tension,[1] laminates with symmetric tapers in three dropped-ply steps subjected to tension[2,3] (helicopter rotor hub application), tensile loading of unsymmetrical tapers in which one side of the laminate is flat[4] (wing skin application), and compression strength of buckling resistant[4,5] and buckling critical laminates.[6] All of these studies have examined failure initiation by delamination in the interfaces surrounding the dropped plies, since experimental evidence[1,2,4] shows delamination as a common mode of failure initiation. Analysis of delamination initiation is either by a mechanics-of-materials approach[2,4] or a fracture-mechanics approach.[1,3,5]

The purpose of this paper is to analyze the response and failure of 25.4-cm-long by 7.62-cm-wide dropped-ply laminated plates tested in flat-end compression.[7] The specimens were fabricated from AS4/3502 graphite/epoxy unidirectional tape. Compression tests were performed on 2.54- and 3.81-cm-wide specimens as well, and these results are discussed in Ref. 4. The specimens of all three widths had sublaminates of two, four, or eight plies terminated in a single step at the midplane of the thick section, such that one surface of the specimen was flat and the opposite surface sloped abruptly to accommodate the change in thickness caused by the dropped plies (unsymmetrical taper) (see Fig. 1). The specimens are $[(\pm 45/0/90)_s, D, (\pm 45/0/90)_s]_T$ laminates, in which the 0-deg fiber direction is parallel to the longitudinal x axis, or load axis, and D denotes the dropped-ply sublaminate layup. Dropped-ply layups are listed in Table 1, as are other experimental data. To assist in monitoring the initiation of delamination, a Questar telescope with an attached camera was used to observe and photograph the edge of the specimens in the vicinity of the dropped plies. A more detailed discussion of the experiments is presented in Ref. 4. Two important observations from the tests[7] on the 7.62-cm-wide specimens form the basis of this paper. First, the compressive load per unit width $\bar{N}_x$ at delamination initiation was less for the wider dropped-ply specimens ($b = 7.62$ cm) than for the narrower specimens ($b = 2.54$ cm), all other things being equal. Second, the wider specimens exhibited a nonlinear response to delamination initiation where the narrower specimens behaved linearly.

Finite Element Analysis

Dropped-Ply Laminate Model

The analyses of this study were performed using a structural analysis software system called the COmputational MEchanics Testbed,[8,9] or COMET. A dropped-ply laminate model was developed that consists of shell elements, solid elements, and transition elements. The shell element used is a nine-node assumed natural strain (ANS) element[10] with five degrees of freedom per node (no drilling rotation), and includes transverse shearing deformation. It is denoted as EX97 in COMET. The solid element used is a 20-node serendipity brick element with three displacement degrees of freedom per node, which is denoted as BR20 in COMET.

The transition element permits connection of a shell element to a stack of brick elements through the thickness of the laminate. Thus, shell nodes do not necessarily lie on the face of the transition element that connects to the shell element as shown in Fig. 2. This transition element was not in the

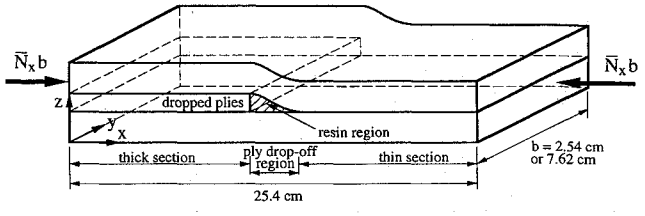

Fig. 1 Schematic of the dropped-ply compression specimens. Width b is either 2.54 cm or 7.62 cm.

Received March 9, 1992; presented as Paper 92-2226 at the AIAA/ASME/ASCE/AHS/ASC 33rd Structures, Structural Dynamics, and Materials Conference, Dallas, TX, April 13–15, 1992; revision received July 17, 1992; accepted for publication July 25, 1992.

*National Research Council Resident Research Associate.

†Associate Professor, Aerospace and Ocean Engineering Department. Senior Member AIAA.

Table 1 Measured data and delamination initiation loads for compression specimens[a] from Ref. 7

Specimen no.	Dropped-ply layup	Average width, cm	Average thin side ply thickness, mm	Average thick side ply thickness, mm	Delamination initiation load, kN/cm
A3, A4, A5	$[0_2]_T$	2.544	0.1264	0.1255	9.013
A7	$[0_2]_T$	7.620	0.1372	0.1367	6.164
B3, B4, B5	$[0_4]_T$	2.546	0.1262	0.1251	6.468
B6	$[0_4]_T$	7.635	0.1372	0.1367	5.989
C3,C4,C5	$[0_8]_T$	2.543	0.1290	0.1270	6.117
C7	$[0_8]_T$	7.623	0.1290	0.1270	5.113
D3,D4, D5	$[\pm 45/0_2]_s$	2.547	0.1271	0.1270	6.725
D6	$[\pm 45/0_2]_s$	7.635	0.1273	0.1270	6.085

[a]All specimens nominally 25.4 cm long with $[(\pm 45/0/90)_s, D, (\pm 45/0/90)_s]_T$ layup, in which D denotes the layup of the dropped plies.

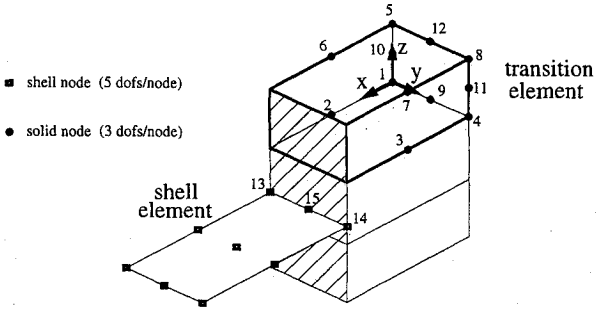

Fig. 2 Connection between the shell element and transition element is made by kinematic assumptions.

COMET library, but was developed as part of this research by degenerating the 20-node solid element as detailed Ref. 11. We designated the transition element TR15, since it has 15 nodes. It has 51 degrees of freedom.

The configuration of the shell, transition, and solid elements in the dropped-ply laminate model is shown in Fig. 3. As shown in this figure, the largest area of the laminate is modeled by the EX97 shell elements, whereas only the region closest to the ply dropoff is composed of solid elements (4% of the total planform area). The length in the x direction of the region of solid elements is 1.016 cm, of which 0.635 cm is on the thick side and 0.381 cm is on the thin side of the dropoff (see Fig. 4). Note that the origin of the x axis is moved to the ply dropoff in Fig. 4, and this will be the convention in the remaining figures. The length of the solid element region along the x axis was selected on the basis of the results in Ref. 4, which indicated that the interlaminar stress gradients for the 2.54-cm-wide specimens were confined within the 1.016 cm length. The solid element region spans the entire width in the y direction of the model.

Symmetry conditions were imposed on x-z plane at $y = b/2$ of the model, i.e., the displacements in the y direction (denoted by v) on this plane of geometric symmetry were set to zero. Although the presence of the ± 45 deg plies does not strictly admit the x-z plane at $y = b/2$ as a plane of symmetry, studies on the full-width model for the laminates in this study showed the influence of asymmetry was negligible.

The prescribed boundary conditions approximate the experimental setup. At the thick end, all nodal displacements and rotations of the shell elements are prescribed to vanish at $x = 0$, except that a uniform x-direction displacement is imposed along with specifying the total axial compressive force. At the thin end, all shell kinematic degrees of freedom are prescribed to vanish at $x = 25.4$ cm. At both the thick and thin ends, the out-of-plane displacements w for the shell elements within the 9.525 mm by $b/2$ area of the grips are prescribed to vanish. Knife edges run along the length of the plate, 3.175 mm inward from the free edge of the laminate. For shell elements, knife-edge conditions are modeled by specifying $w = 0$ along this line. For solid elements, a clamping action of the knife edges was simulated by specifying $w = 0$ at the bottom ($z = 0$) knife-edge support line and by specifying a small pinching displacement $w = -1 \times 10^{-4}h$ at the top ($z = h$) knife-edge support line on the thick side, where h denotes the laminate thickness on the thick side. The material properties used for the model are given in Table 2, and are the same as those used in Ref. 4.

The model consists of 24 EX97 shell elements, 15 TR15 transition elements, and 45 BR20 brick elements. There are 126 shell nodes, 684 solid element nodes, and 2361 active degrees of freedom. The mesh for a longitudinal cross section in the region of the solid elements at the ply dropoff is shown in Fig. 4. There are 12 BR20 elements in the x direction, 3 elements in the y direction, 3 elements through the thickness in the thick section, and 2 elements through the thickness in the thin section shown in Fig. 4. To have only one element span the thickness of a sublaminate, it is necessary to homogenize the thickness variation of the elasticity matrix from each ply in the sublaminate. This is done in the LAU processor in COMET, and a theory for this type of homogenization is given in Ref. 12. The element ahead of the dropoff in the taper is composed of pure resin, with material properties given in Table 2.

Nonlinear Formulation in COMET

The geometrically nonlinear finite element analysis is based on the total Lagrangian formulation, in which the fully nonlinear Green-Lagrange strain-displacement relations are employed for the solid and transition elements, and a simplified approximation of the nonlinear Lagrange strain tensor is used for the shell elements (Ref. 9, Chap. 5). The modified Newton-Raphson iterative procedure is used to solve for the nodal displacements at equilibrium under a fixed applied load. The matrices for the geometrically nonlinear analysis for the solid and transition elements were not available in the COMET processors, so they were developed and implemented as part of this research.[11] Crisfield's arc-length strategy is used in COMET to continue along a nonlinear equilibrium path in the load-displacement space.

Delamination Initiation Analysis

In a given equilibrium state, the interlaminar stress components are computed in the upper and lower interfaces (Fig. 4) surrounding the dropped plies. These stress components are computed at discrete x-y points in the interfacial plane by interpolating like stress components between the Gauss point immediately above the interface and the Gauss point immediately below the interface. (The x-y locations of the Gauss points in the elements adjacent to the interface are the same and only their z coordinates are different.) From the interlaminar stresses, a dimensionless quadratic failure index F is computed from[13]

$$F = (\tau_{zx}/Z^{S1})^2 + (\tau_{zy}/Z^{S2})^2 + (\tau_{zz}/Z^T)^2, \qquad \tau_{zz} > 0 \quad (1)$$

in which τ_{zx} and τ_{zy} are the interlaminar shear stresses, τ_{zz} is the interlaminar normal stress, and Z^{S1}, Z^{S2}, and Z^T are the

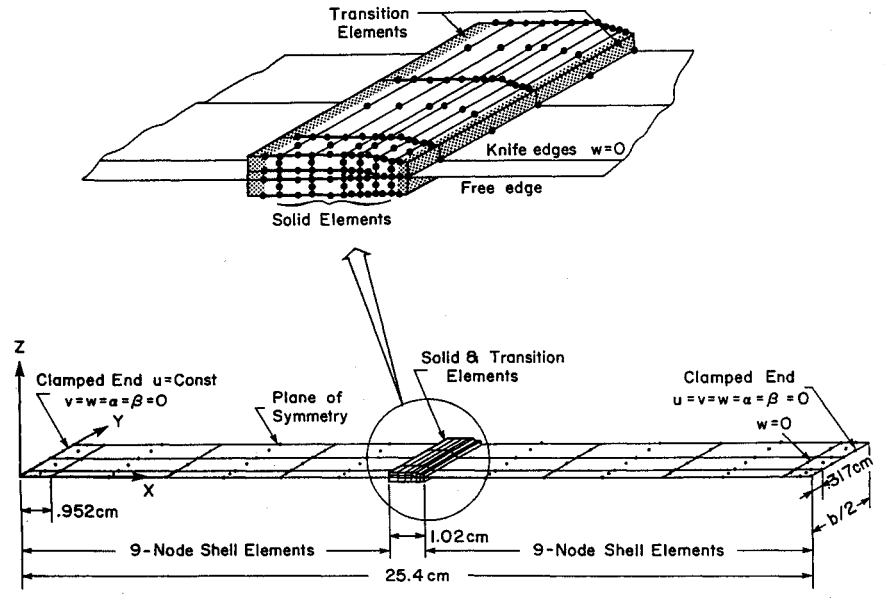

Fig. 3 Configuration of the shell, transition, and solid elements in the dropped-ply laminate model.

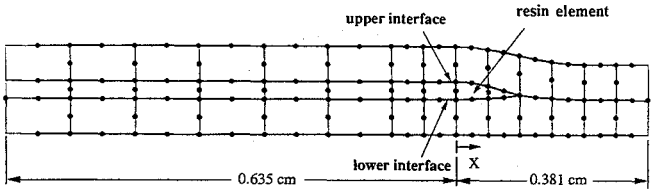

Fig. 4 Detail of the finite element mesh at the ply dropoff showing the solid elements in the longitudinal and thickness directions.

interlaminar strength allowables. The interlaminar strength allowables assumed for AS4/3502 are given in Table 2.

In the delamination initiation studies of Refs. 2, 13, and 14, average values of the interlaminar stresses are computed and used in Eq. (1), or in a similar criterion, rather than the peak values at the stress riser or dropoff. An elasticity solution for an effective modulus model may have a singularity at a discontinuity, and a finite element solution may show increasing peak magnitudes for increasingly finer meshes. Thus, evaluation of the stresses at a discontinuity in numerical solutions to an effective modulus model is not meaningful, whereas averaging the stresses is meaningful if the distribution of the stresses in the vicinity of the stress singularity are reasonably well represented. This type of "average stress criterion" was introduced by Whitney and Nuismer[15] to predict the ultimate failure of notched laminates and to explain the hole-size effect. These authors[15] also introduced a "point stress criterion" that predicts laminate failure when the stress a fixed distance d_0 in front of the stress riser (notch) reaches the unnotched strength of the material. The averaging distance and d_0 are considered material parameters to be determined from tests. Although the point stress criterion has not been extended to delamination initiation by previous researchers, we assume it will serve the same purpose as the averaging criterion. That is, the point value of F evaluated at some fixed distance from the stress riser or dropoff is a reasonable estimate of the severity of the interlaminar stress distribution near this likely singularity. We designate this distance as the characteristic distance d. In contrast to the one-dimensional dependence of interlaminar stress distributions in Refs. 2, 13, and 14, the interlaminar stress distributions in the present study depend on coordinates x and y in a given interface, so that the evaluation of the failure index at a fixed distance from the dropoff implies F is a function of y.

Table 2 Material properties and strength allowables assumed for AS4/3502 graphite/epoxy unidirectional tape and neat resin

	AS4/3502 graphite/epoxy		
E_1	126 GPa	18.5 Msi	Young's modulus in fiber direction
E_2	11.3 GPa	1.64 Msi	Young's modulus in matrix direction
E_3	11.3 GPa	1.64 Msi	Young's modulus in thickness direction
ν_{12}	0.3		Major Poisson's ratio in 1-2 plane
ν_{13}	0.3		Major Poisson's ratio in 1-3 plane
ν_{23}	0.3		Poisson' ratio in 2-3 plane
G_{12}	6.0 Gpa	0.87 Msi	Shear modulus in 1-2 plane
G_{13}	6.0 GPa	0.87 Msi	Shear modulus in 1-3 plane
G_{23}	3.38 GPa	0.49 Msi	Shear modulus in 2-3 plane
	Neat resin		
E	3.45 GPa	0.50 Msi	Young's modulus
ν	0.41		Poisson's ratio
G	1.34 GPa	0.195 Msi	Shear modulus
	Interlaminar strengths		
Z^{S1}	93.1 MPa	13.5 ksi	Longitudinal shear strength
Z^{S2}	93.1 MPa	13.5 ksi	Transverse shear strength
Z^T	52.0 MPa	7.54 ksi	Tensile strength

Characteristic Distance d

From the linear analysis of the 2.54-cm-wide specimen of a given dropped-ply layup, the distribution of the failure index in the upper and lower interface is computed at the experimental delamination initiation load. The interface with the largest magnitude of the index is selected as critical, and the $F = 1$ contour in this interface is located. The characteristic distance d is determined as the largest x-direction distance from the dropoff at $x = 0$ to the contour of unit value.

Failure Criterion

From the nonlinear analysis of the 7.62-cm-wide specimen, the failure index F is computed along the line $x = -d$, $0 \le y \le b/2$ in the critical interface. This line is called the characteristic line and runs parallel to the ply termination. The first value of the applied compressive load at which $F = 1$ on this characteristic line is defined to cause failure initiation by delamination in the interface. Failure is considered to occur somewhere between the dropoff and the characteristic line, and not necessarily at the point (designated the characteristic point) where the unit contour and characteristic line touch. However, the shifting of the characteristic point for different dropped-ply layups provides qualitative evidence as to the movement of the delamination initiation site.

Results and Discussion

Mesh Refinement

A comparison of the interlaminar normal stress distributions in the upper interface at $y = b/2$ from Ref. 4 and the present study are shown in Fig. 5. Stresses plotted in Fig. 5 are from linear analyses of a laminate 2.54-cm wide, with a $[0_4]_T$ dropped-ply layup, and at a compressive load intensity $\bar{N}_x = 508.5$ N/cm. Stresses for mesh 1 refer to the discretization shown in Fig. 4, whereas stresses for mesh 2 consist of 19 BR20 elements in the x direction rather than the 12 shown in Fig. 4. The interlaminar stresses computed from the two

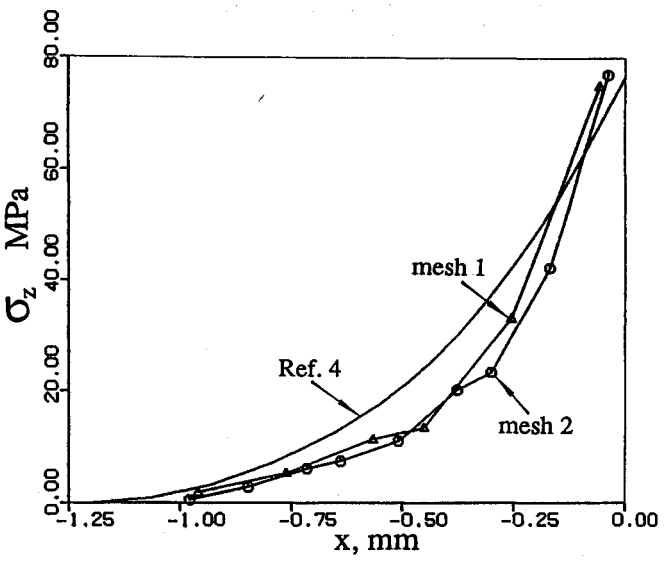

Fig. 5 Longitudinal distribution of the interlaminar normal stress along the center in the upper interface for a 2.54-cm-wide, $[0_4]_T$ dropped-ply laminate at 508.5 N/cm compression.

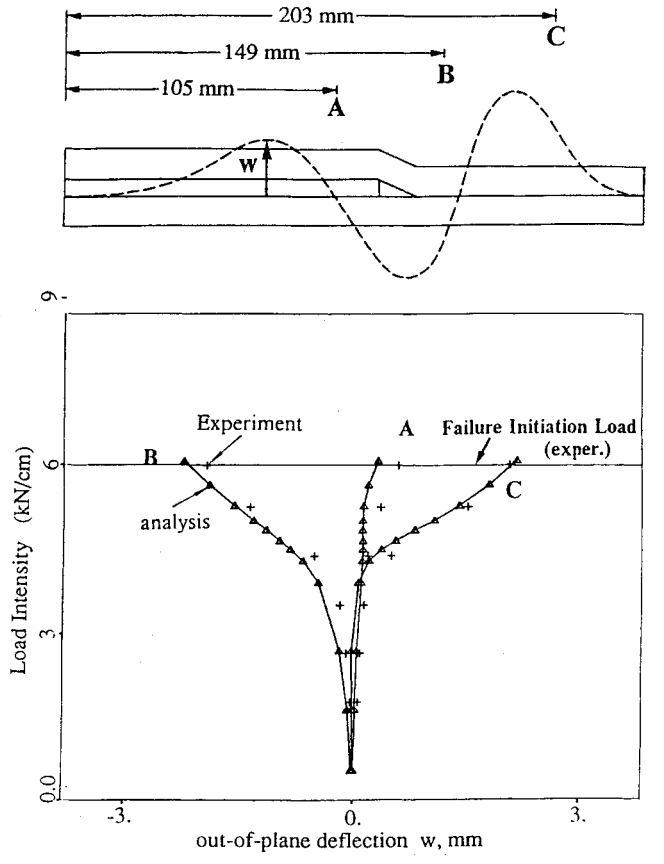

Fig. 6 Comparison of the out-of-plane displacements of specimen B6 at three longitudinal locations to the nonlinear analysis.

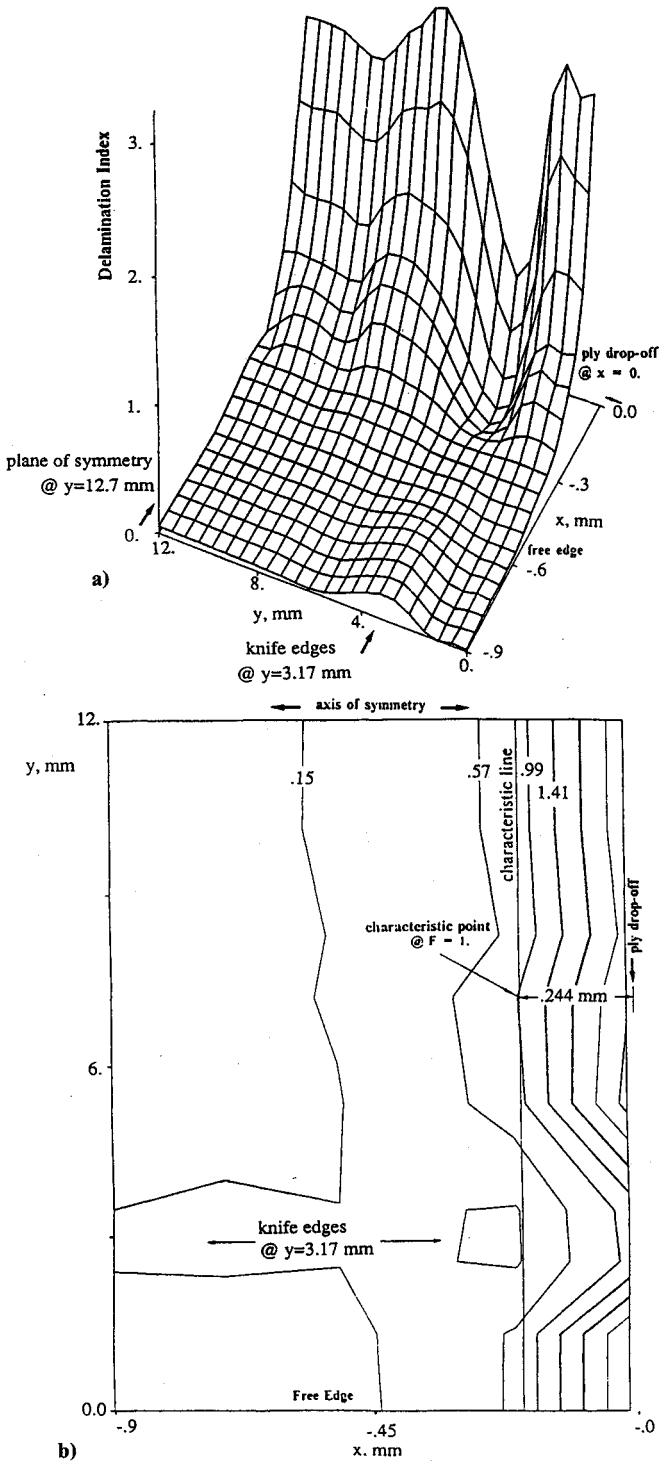

Fig. 7 Distribution of the failure index in the upper interface of the 2.54-cm-wide $[0_4]_T$ dropped-ply laminate at the failure initiation load of the experimental specimen from linear analysis: a) relief map; and b) contour plot.

meshes for the fully three-dimensional model in this work compare favorably to the stresses from the mathematically two-dimensional model of Ref. 4 (generalized plane strain in the x-z plane). Since the difference between the results for mesh 1 and those for mesh 2 are small, we selected mesh 1 for the results presented here because it has fewer degrees of freedom.

Delamination Analysis of $[0_4]_T$ Specimens

The out-of-plane displacement w of specimen B6 ($b = 7.62$ cm) as measured by displacement transducers at three longitudinal positions at $y = b/2$ and at several applied compressive

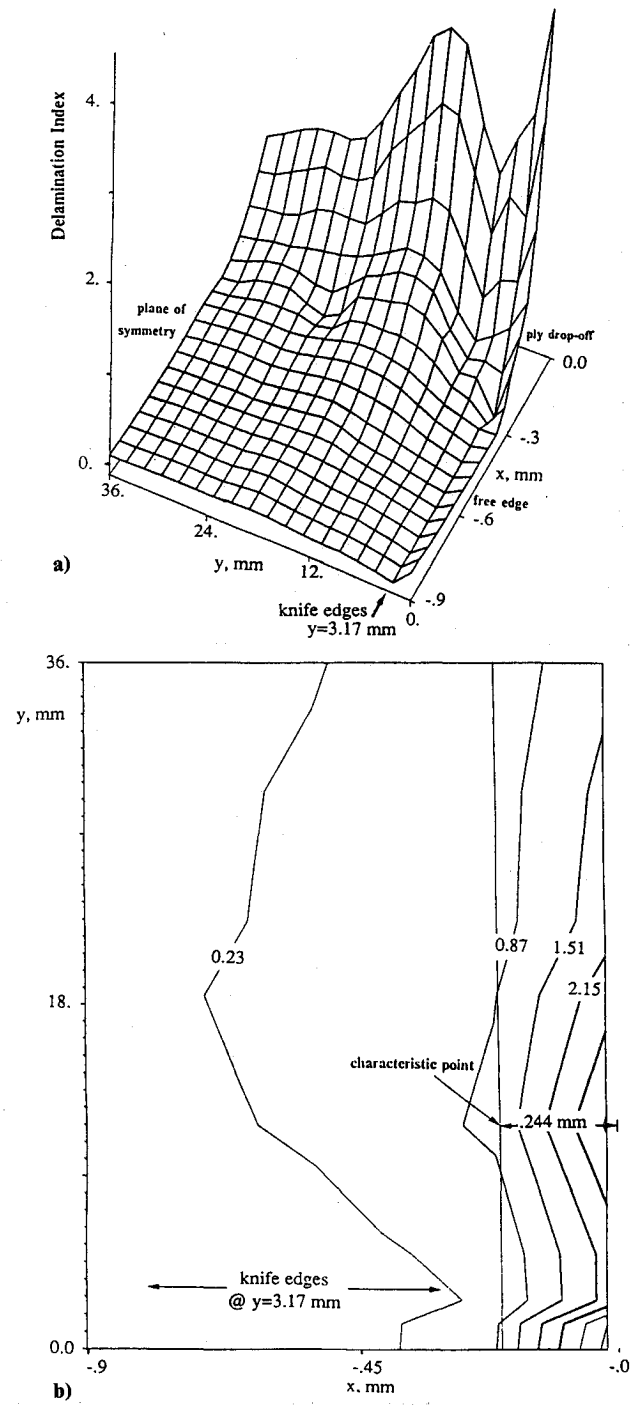

Fig. 8 Distribution of the failure index in the upper interface of the 7.62-cm-wide $[0_4]_T$ dropped-ply laminate at 6.09 kN/cm compression from nonlinear analysis: a) relief map; and b) contour plot.

load magnitudes are indicated by crosses in the plot in Fig. 6. Triangles indicate predictions from the nonlinear analysis on this plot, and the triangles for the displacements at a given longitudinal position are connected by a solid line. The data in Fig. 6 show the analysis correlates well with the experiment for this specimen.

Using the average dimensional data at the average failure load for the three 2.54-cm-wide specimens B3, B4, and B5 (Table 1), the distribution of the failure index in the upper and lower interfaces is computed from a linear analysis. The distribution of the failure index F in the upper interface is plotted as a relief map above the interfacial plane in Fig. 7a. A smaller maximum magnitude of F occurs in the lower interface, thus the upper interface is critical. High elevations and steep slopes at $x = 0$ depicted in Fig. 7a result from the interlaminar stress concentration at the dropoff. A valley along the knife-edge support line results from the clamping action imposed on the laminate by the knife edges. The clamping action reduces the tensile interlaminar normal stresses, or peel stresses, in the interface along the knife-edge support line. At $x = -0.9$ mm near the knife-edge support line, a small hill appears due to compressive interlaminar normal stresses. A precise definition of the delamination index should not include compressive interlaminar normal stresses but they are included in the results presented in Fig. 7a. (See Refs. 13 and 14 for criteria which include compressive interlaminar normal stress.) This small hill does not affect the delamination analysis for this particular problem since the highest elevations are caused by the peel stresses near $x = 0$. Contour lines of index F in the upper interfacial plane are shown in Fig. 7b, and the characteristic distance to the unit contour is determined to be 0.244 mm.

Although the data is not presented in this paper, a nonlinear analysis of the 2.54-cm-wide dropped-ply model showed that the geometric nonlinearity had an insignificant effect on its response. Thus, the distribution of index F from the linear analysis shown in Fig. 7a remains valid even if geometric nonlinearity were included in the analysis. The peak value of F near the free edge is slightly less than the peak value of F near the center of the laminate. This distribution of the failure index in Fig. 7a shows why the generalized plane strain analysis in the x-z plane of Ref. 4, an analysis which neglects free edge effects, was a reasonable mathematical model. Free-edge effects are not quite as severe as the stress concentration at the interior of the laminate in the linear response analysis.

The distribution of the delamination index F for the 7.62-cm-wide specimen B6 from the nonlinear analysis is plotted as a relief map above the upper interfacial plane in Fig. 8a at $\bar{N}_x = 6.094$ kN/cm, The distribution of the index from the nonlinear analysis in Fig. 8a bears some resemblance to the distribution from the linear analysis in Fig. 7a. An important topographical distinction is that the peak elevations at the center of the laminate are lower than the peak elevations near the knife edges in the relief from nonlinear analysis compared to the relief from linear analysis. The implication of this topographical distinction is that the interlaminar stress concentration at the ply dropoff in the interior is less than at the dropoff near the knife edge. The shift in peak elevations toward the knife edge in the nonlinear analysis is further reflected by the closer relative proximity of the characteristic point to the knife edge with respect to the linear analysis results (compare Figs. 8b and 7b). The elevation at the characteristic point in Fig. 8b is 1.15, which indicates that $\bar{N}_x = 6.094$ kN/cm exceeds the delamination initiation load. The previous load step in the nonlinear analysis was below the delamination initiation load, so interpolation between these load values yielded a predicted delamination initiation load of 5.814 kN/cm. This predicted failure load is 2.9% low relative to the experimental value (see Table 3).

Delamination Analysis of the Remaining Specimens

The procedure for the delamination analysis of the remaining specimens is the same as just outlined for the $[0_4]_T$ dropped-ply specimens. The results are tabulated in Table 3.

Table 3 Characteristic distance, delamination initiation load predicted from nonlinear analysis, and experimental delamination initiation load for the 7.62-cm-wide dropped-ply compression specimens

Specimen no.	Characteristic distance,[a] mm	Delamination initiation load, kN/cm		Discrepancy of predicted failure load with respect to experiment
		Predicted	Experiment	
A7	0.2362	6.409	6.164	4.0% high
B6	0.2438	5.814	5.989	2.9% low
C7	0.2769	4.938	5.113	3.4% low
D6	0.3200	5.551	6.085	8.8% low

[a]Determined from a linear analysis on corresponding 2.54-cm-wide specimen.

Nonlinear analyses of the $[0_8]_T$ dropped-ply specimen C7 and the $[\pm 45/0_2]_s$ dropped-ply specimen D6 showed the characteristic point moved to the free edge in the upper interface at delamination initiation. The characteristic point from the nonlinear analyses of the two thinner dropped-ply specimens occurred at a location inboard of the knife edge. A separate characteristic distance measured inward from the free edge may be needed in cases of delamination initiation predicted at the free edge. However, we had no experimental data from the 2.54-cm-wide specimens to compute a characteristic distance from the free edge, because the linear analysis confirmed that the 2.54-cm-wide specimens delaminated due to the ply dropoff and not due to the free-edge effect.

The delamination initiation loads for the 0-deg specimens analyzed in this study are shown in Fig. 9, which is a plot of load vs number of dropped 0-deg plies. Failure loads from the experiment with $b = 2.54$ cm, the experiment with $b = 7.62$ cm, the linear analysis with $b = 7.62$ cm, and from the nonlinear analysis with $b = 7.62$ cm, are each connected by solid lines in Fig. 9 to show the trends for the 0-deg dropped-ply layups. The experimental data show the compression strength of the 7.62-cm-wide specimen is less than the compression strength for the corresponding 2.54-cm-wide specimen, and that the compression strength decreases for an increasing number of dropped plies for both specimen widths. The analytical predictions of the failure loads for the 7.62-cm-wide specimens from the nonlinear analysis are very good, and the analytical results from the linear analysis for the 7.62-cm-wide specimens are in very poor agreement with respect to the experiment.

The largest decrease in compression strength between the 2.54-cm-wide specimens and the 7.62-cm-wide specimens occurs for the $[0_2]_T$ dropped-ply layup. That is, the compressive failure load for the 7.62-cm-wide specimen A7 is 31.6% less than the average failure load of the corresponding 2.54-cm-wide $[0_2]_T$ specimens A3, A4, and A5 (see Tables 1 and 3). For the $[0_4]_T$ layup the decrease is 7.4% for the 7.62-cm-wide specimen relative to the 2.54-cm-wide specimens, and for the $[0_8]_T$ layup the corresponding decrease is 16.4%.

Influence of the Geometric Nonlinearity on the Stress Concentration

The mechanism for the lower strength of the wider dropped-ply specimens relative to their narrower counterparts is explained by the geometric nonlinearity in the response of the former that is insignificant in the latter. The large amplitude out-of-plane displacements in the center of the laminate due to the geometrically nonlinear response (postbuckling) decrease rapidly to zero in a narrow region near the knife-edge support, causing severe displacement gradients to occur near the knife edge. These severe out-of-plane displacement gradients at the dropped-ply site near the knife edge increase the interlaminar stress concentration beyond what occurs in the center of the laminate. This mechanism of interlaminar stress redistribution at the dropped-ply site due to postbuckling is similar to the redistribution of the in-plane stress resultant in longitudinally compressed flat rectangular plates having supported edges all around. For compressively loaded flat plates loaded beyond buckling, the in-plane axial stress resultant at the center of the plate is decreased due to bending in postbuckling at the expense of increased resultants at the two supported edges which are not subjected to compressive load, because the edge region of the plate is prevented from bending by these supports.

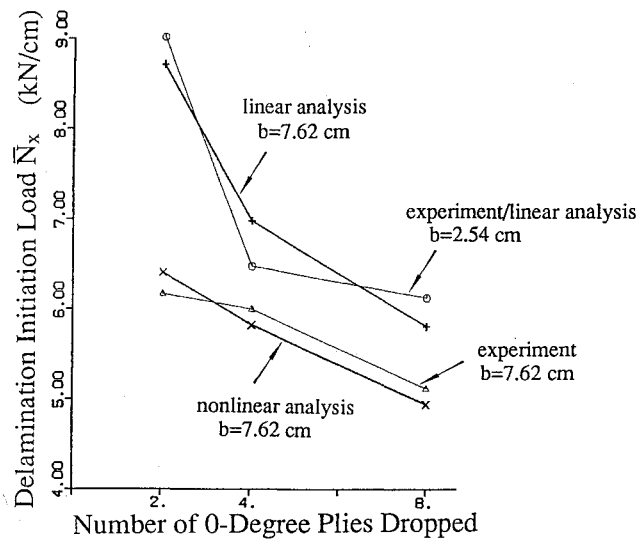

Fig. 9 Compressive loads to initiate delamination for the dropped-ply specimens compared to analytical predictions.

For the three 0-deg dropped-ply layups (Fig. 9), the largest decrease in compression strength due to the geometrically nonlinear response occurs for the thinnest layup; i.e., $[0_2]_T$. It is reasonable to expect that a fewer number of dropped plies means a more benign taper and lower interlaminar stress concentration at the dropoff. Likewise it is reasonable to expect a thinner laminate to have larger bending amplitudes in postbuckling. Consequently, larger displacement gradients near the knife edge must be occurring for the $[0_2]_T$ dropped-ply layup than for the two thicker 0-deg dropped-ply layups, and so the interlaminar stress concentration due to the geometric nonlinear response is more severe for this case.

Failure Methodology

The achievement of excellent correlation between analytical predictions of the compressive strength and the experiments for the 7.62-cm-wide dropped-ply specimens results, in large part, from determining the characteristic distance from tests on the 2.54-cm-wide specimens. Ideally, the characteristic distance should be a material parameter independent of the laminate layup. However, the limited number of laminates considered in this study show that the characteristic distance (Table 3) to be about 1.7 to 2.5 ply thicknesses depending on the dropped-ply layup. The computed characteristic distances shown in Table 3 for the three 0-deg dropped-ply layups have a coefficient of variation of -6.4 to 9.8% with respect to their average value, and this variation seems reasonable when compared to averaging distances reported in Ref. 13 for AS1/3501-6 graphite/epoxy laminates. Since we were interested in comparing linear vs nonlinear response for a fixed dropped-ply layup, further investigation of relation of the characteristic distance to the dropped-ply layup was not pursued.

Concluding Remarks

The development of a transition element to connect shell and solid elements in COMET[9] permitted a relatively coarse finite element model to capture the fully three-dimensional, geometrically nonlinear response in the vicinity of the dropped plies. This analysis confirms that the influence of the geometric nonlinearity on the response of the 2.54-cm-wide dropped-ply laminate is insignificant, but this nonlinearity is a significant effect in the response of its 7.62-cm-wide counterpart. The geometrically nonlinear response, or postbuckling, causes a redistribution and intensification of the severe interlaminar stress gradients occurring at the dropoff to a location closer to the knife edge (see Fig. 8a). This redistribution occurs because the large bending amplitudes associated with postbuckling are suppressed over a small region near the knife edge, which increase the displacement gradients (or strains) occurring there. The large bending amplitudes in the center of the laminate have less influence on the interlaminar stress concentration because the waveforms in postbuckling tend to flatten out across the width, and hence the displacement gradients are expected to be less than near the knife edge.

The predicted compression strengths for delamination initiation of the 7.62-cm-wide dropped ply laminates are in very good agreement with experimental measurements (Table 3). The influence of the geometric nonlinearity on the interlaminar stress concentration is highlighted by the fact that the largest decrease in compressive strength occurs for the thinnest dropped-ply configuration; i.e., the $[0_2]_T$ dropped-ply layup

(Fig. 9). A delamination initiation methodology based on a existing quadratic interlaminar failure index,[13] Eq. (1), but evaluated at a characteristic distance from the stress riser (ply dropoff), is hypothesized. The success of this failure methodology is based on having test data to determine the characteristic distance, which in this work was available from the 2.54-cm-wide specimens.

Acknowledgments

This research was supported under NASA Grant NAG1-537, and James H. Starnes Jr., Head, Aircraft Structures Branch, NASA Langley Research Center, is the technical monitor. We gratefully acknowledge the many fruitful technical discussions with James Starnes. In addition, we acknowledge Jerrold Housner, Christine Lotts, and Mohammad Aminpour of the Computational Mechanics Branch at the NASA Langley Research Center for their assistance with the COMET software system.

References

[1]Wisnom, M. R., "Delamination in Tapered Unidirectional Glass Fibre-Epoxy Under Static Tension Loading," *Proceedings of the AIAA/ASME/ASCE/AHS/ASC 32nd Structures, Structural Dynamics, and Materials Conference, Part 2* (Baltimore, MD), AIAA, Washington, DC, April 1991, pp. 1162–1172 (AIAA Paper 91-1142-CP).

[2]Fish, J. C., and Lee, S. W., "Tensile Strength of Tapered Composite Structures," *Proceedings of the AIAA/ASME/ASCE/AHS/ASC 29th Structures, Structural Dynamics, and Materials Conference, Part 1* (Williamsburg, VA), AIAA, Washington, DC, April 1988, pp. 324–333 (AIAA Paper 88-2252).

[3]Salpekar, S. A., Raju, I. S., and O'Brien, T. K., "Strain Energy Release Rate Analysis of Delamination in a Tapered Laminate Subjected to Tension Loading," *Proceedings of the American Society for Composites,* 3rd Technical Conf. (Seattle, WA), Technomic Publishing, Lancaster, PA, 1988, pp. 642–654.

[4]Curry, J. M., Johnson, E. R., and Starnes, J. H., Jr., "Effect of Dropped Plies On the Strength of Graphite-Epoxy Laminates," *AIAA Journal,* Vol. 30, No. 2, 1992, pp. 449–456.

[5]Trethewey, B. R., Jr., Gillespie, J. W., Jr., and Wilkins, D. J., "Interlaminar Performance of Tapered Composite Laminates," *Proceedings of the American Society for Composites,* 5th Technical Conf. (E. Lansing, MI), Technomic Publishing, Lancaster, PA, 1990, pp. 361–372.

[6]DiNardo, M. T., and Lagace, P. A., "Buckling and Postbuckling of Laminated Composite Plates with Ply Dropoffs," *AIAA Journal,* Vol. 27, No. 10, 1989, pp. 1392–1398.

[7]Curry, J. M., Johnson, E. R., and Starnes, J. H., Jr., "Effect of Ply Drop-Offs on the Strength of Graphite-Epoxy Laminates," Center for Composite Materials and Structures, Virginia Polytechnic Inst. and State Univ., CCMS-86-07 and VPI-E-86-27, Blacksburg, VA, Dec. 1986.

[8]Knight, N. F., Jr., Lotts, C. G., and Gillian, R. E., "Computational Structural Mechanics Methods Research Using an Evolving Framework," *Proceedings of the AIAA/ASME/ASCE/AHS/ASC 31st Structures, Structural Dynamics, and Materials Conference, Part 2* (Long Beach, CA), AIAA, Washington, DC, April 1990, pp. 618–637 (AIAA Paper 90-1145-CP).

[9]Stewart, C. B., "The Computational Structural Mechanics Testbed User's Manual," NASA TM 100644, Oct. 1989.

[10]Park, K. C., Pramono, E., Stanley, G. M., and Cabiness, H. A., "The ANS Shell Elements: Earlier Developments and Recent Improvements," *Analytical and Computational Models of Shells,* CED-Vol. 3, edited by A. K. Noor, T. Belytschko, and J. C. Simo, American Society of Mechanical Engineers, New York, 1989, pp. 217–239.

[11]Dávila, C. G., and Johnson, E. R., "Delamination Initiation in Postbuckled Dropped-Ply Laminates," Center for Composite Materials and Structures, Virginia Polytechnic Inst. and State Univ., CCMS-91-24 and VPI-E-91-23, Blacksburg, VA, Dec. 1991.

[12]Sun, C. T., and Li, Sijan, "Three-Dimensional Effective Elastic Constants for Thick Laminates," *Journal of Composite Materials,* Vol. 22, July 1988, pp. 629–639.

[13]Brewer, J. C., and Lagace, P. A., "Quadratic Stress Criterion for Initiation of Delamination," *Journal of Composite Materials,* Vol. 22, Dec. 1988, pp. 1141–1155.

[14]Kim, R. Y., and Soni, S. R., "Failure of Composite Laminates due to Combined Interlaminar Normal and Shear Stresses," *Composites' 86: Recent Advances in Japan and the United States,* edited by K. Kawata, S. Umekawa, and A. Koybayshi, Japan Society for Composite Materials, Japan, 1986, pp. 341–350.

[15]Whitney, J. M., and Nuismer, R. J., "Stress Fracture Criteria for Laminated Composites Containing Stress Concentrations," *Journal of Composite Materials,* Vol. 8, July 1974, pp. 253–265.